A quasi-Monte Carlo solver for thermal radiation in participating media

Joseph Farmer[a], Somesh Roy[a,*]

[a]*Department of Mechanical Engineering, Marquette University, Milwaukee, Wisconsin, USA*

Abstract

The Monte Carlo (MC) method is the most accurate method for resolving radiative heat transfer in participating media. However, it is also computationally prohibitive in large-scale simulations. To alleviate this, this study proposes a quasi-Monte Carlo (QMC) method for thermal radiation in participating media with a focus on combustion-related problems. The QMC method employs low-discrepancy sequences (LDS) in place of the traditional random numbers. Three different low-discrepancy sequences – Sobol, Halton, and Niederreiter – were examined as part of this work. The developed QMC method was first validated against analytical solutions of radiative heat transfer in several one-dimensional configurations. Then it was extended to three-dimensional practical combustion configurations. The results from QMC and traditional Monte Carlo are compared against benchmark solutions for each cases. It is shown that the error of the predicted radiation field from QMC is lower than an equivalent MC simulation. The computational cost of QMC was also found lower than MC due to the avoidance of requirement of several statistical runs for traditional Monte Carlo methods alongside achieving the reduction in error. In conclusion, significant improvements in computational costs and accuracy seen in the QMC method makes it an attractive alternative to traditional Monte Carlo methods in high-fidelity simulations.

Keywords: Radiation, Monte Carlo, Quasi-Monte Carlo, Low-discrepancy sequence, Combustion

*Corresponding author

Email addresses: joseph.farmer@marquette.edu (Joseph Farmer), somesh.roy@marquette.edu (Somesh Roy)

1. Introduction

Radiative transfer through participating media is a complex problem because of the non-local, non-linear nature of the transport. This is further complicated by the nongray properties of the participating media. The spectral radiative transfer equation (RTE), shown in Eqn. 1, governs radiative heat transfer in nongray participating media.

$$\frac{dI_\eta}{ds} = \hat{s} \cdot \nabla I_\eta = \kappa_\eta I_{b\eta} - \beta_\eta I_\eta + \frac{\sigma_{s\eta}}{4\pi} \int_{4\pi} I_\eta(\hat{s}) \Phi_\eta(\hat{s}_i, \hat{s}) d\Omega_i, \tag{1}$$

The spectral RTE is a five-dimensional (three spatial, two directional) integro-differential equation for radiative intensity, I_η, that includes influence from emission, absorption, and scattering. Here the subscript η denotes the spectral nature of the equation, *i.e.*, it is valid for one single wavenumber η; I_b is blackbody radiative intensity (Planck function), κ is absorptivity of the medium, β is extinction coefficient, σ_s is scattering coefficient, $\Phi(\hat{s}_i, \hat{s})$ is the scattering phase function between ray directions $\hat{s}_i$ and $\hat{s}$, and Ω_i represents solid angle. Radiative properties of the medium (κ, σ, β and Φ) vary with wavenumber (η) and thermodynamic states in a highly nonlinear manner.

The difficulty to resolve the RTE exactly led to the development of many approximations for thermal radiation and to the RTE. The simplest approximation is the optically thin (OT) assumption, which does not require to solve the RTE and considers that the media only emits radiation but does not absorb or scatter. Among the more rigorous approximate RTE solution approaches arguably the two most popular methods – the discrete ordinate method (DOM) and the spherical harmonics method (P_N) – approximate the RTE to a set of partial differential equations (PDEs). In the DOM, the radiative intensity over the entire solid angle is discretized directionally to produce a set of simultaneous first-order PDEs from the RTE. In the spherical harmonics method, the intensity is represented in terms of a two-dimensional Fourier series made of position-dependent intensity coefficients and spherical harmonics represented in terms of associated Legendre polynomial. The order N of the spherical harmonics (and hence P_N) represents how many terms of the Fourier series is retained in the numerical solution. Further details of these methods can be found in radiation textbooks [*e.g.*, 1, 2, etc.]. The DOM suffers from some numerical issues, such as ray effect and false scattering, that makes use of DOM in arbitrarily fine resolution numerically

expensive [3, 4]. On the other hand, P_N methods becomes numerically very involved very quickly with the increase in the order (N). Lower-order P_N methods, while computationally cheap, can be grossly inaccurate, specifically in presence of strong intensity gradients. Additionally, complex boundaries are difficult to handle in both methods.

Monte Carlo-based methods, on the other hand, are the most accurate and robust solution methods for RTE. The family of Monte Carlo methods used to solve thermal radiation problems are often referred as photon Monte Carlo (PMC) because the radiative transport is accounted by tracking emission and absorption of photon bundles (sometimes also called "rays") containing a finite amount of energy. As with any Monte Carlo methods, the statistical solution approaches to the exact solution of RTE when sufficiently large number of photons are tracked. However, this comes with a heavy penalty of computational cost. Computational cost of PMC scales almost linearly with the number of rays used in the simulation, whereas the statistical error scales inversely with the square root of the number of rays. Typically a PMC simulation can take orders of magnitude more computational effort than a lower order P_N or DOM calculation [5]. Therefore, Monte Carlo solvers are impractical to use in large-scale simulations, and often only used to generate benchmark solution.

A complete solution of RTE requires supplementary models to tackle the spectral nature of the RTE. This necessitates use of spectral models. Development of accurate and efficient spectral model is an active field of research. Some commonly available spectral models include weighted sum of grey gas (WSGG), full-spectrum k-distribution (FSK), multiscale/multigroup FSK model, spectral line weighted-sum-of-gray-gases (SLW) models, l-distribution model, statistical narrow band (SNB) methods, absorption distribution function model with fictitious gases (ADFFG), multiscale Malkmus model (MSM), line-by-line model (LBL) model, etc [*e.g.*, 6, 7, 8, 9, 10, 11, 12, 13, 14, 15, 16, 17, 18, 19, 20, 21]. The accuracy and complexity of spectral models vary significantly. The accuracy of an RTE solver is affected by accuracy of spectral model used with it. Several studies have compared accuracy and efficiency of different spectral models with different RTE solvers in various contexts [*e.g.*, 22, 23, 24, 25, 26].

Due to the stochastic nature, the complexity of spectral model does not significantly affect the computational efficiency of PMC. Therefore, considering the high computational cost, an accurate

spectral model is often preferred in PMC. In the context of the RTE in a combustion system, a solution using a line-by-line spectral model with Monte Carlo solver (PMC/LBL) is generally considered one of the most accurate solution approaches. However, it is possible to use PMC with any other sufficiently accurate (*e.g.*, FSK or SLW models, or *l*-distribution models, etc.) spectral model. For example, PMC has been used with variants of FSK model with good accuracy and efficiency [27, 28]. There has also been some recent developments in calculating radiative transfer directly from spectroscopic databases via a line-sampling Monte Carlo approach [29]. It is noted here that the scope of the current work is not to explore different spectral models and their impacts on PMC, rather to propose a new variant of Monte Carlo-based RTE solver. For this reason, in this work, we only use LBL spectral model.

The current work proposes an approach of utilizing low-discrepancy sequences to develop a more efficient Monte Carlo method without sacrificing any accuracy. The idea of using low-discrepancy sequence in Monte Carlo methods has been used in different domains of computations from financial applications [30] to computer graphics [31]. These methods are termed as quasi-Monte Carlo (QMC) [32]. The use of QMC in thermal radiation problem, however, is very limited and mostly restricted to surface transfer and atmospheric radiation [*e.g.*, 33, 34, 35, 36, 37, etc.]. In this work we extend this approach to thermal radiation in participating media. Very recently researchers have compared various Monte Carlo methods including a QMC for combustion simulations [38]. To the best knowledge of the authors, other than the few works cited above, there has not been many work in exploring and systematically validating and verifying efficacies of QMC in solving radiation in participating media.

In computational simulations, the choice of RTE solver is dictated by the importance of thermal radiation in the problem under consideration. Typically, thermal radiation is important in most high temperature applications. The use case considered in this study is that of combustion, which contains highly nonuniform distribution of nongray participating media. In combustion applications, the effect of radiation comes in terms of a source term in the energy conservation equation and in the heat loss at the boundary. Although considerable development has taken place on DOM and P_N methods with combustion simulation in mind, thermal radiation is often either neglected or oversimplified in combustion applications mainly because of the added computational expense

despite the importance thermal radiation in combustion applications [*e.g.*, see 39, and references therein]. Although the configurations discussed in this work is relevant for combustion, the approach presented here can be easily extended to other application domains involving participating media such as biomedical imaging, photodynamic therapy, radiation therapy, etc. [40, 41].

In the next section a brief overview of conventional Monte Carlo method of thermal radiation is presented followed by a section on the description of the proposed quasi-Monte Carlo method. The results section first reports validation of QMC followed by its comparison with conventional Monte Carlo method in different combustion configurations. Finally the key findings are summarized in the conclusion. In the rest of the document the words photon Monte Carlo (PMC) and Monte Carlo (MC) are used interchangeably to represent conventional Monte Carlo method for radiation.

2. Monte Carlo method for radiation in participating media

In the photon Monte Carlo (PMC) method the radiative transport is accounted for by emitting and tracing a statistically meaningful sample of representative photons (rays). Each ray starts with a finite amount of energy, has a specific wavenumber and assumed to propagate along a line in a specific direction. A ray's (denoted by its index j) origin (x_j, y_j, z_j), propagation direction (θ_j, ϕ_j), and the wavenumber (η_j) are determined via importance sampling of independent random numbers according to probability distributions [1]. In the conventional approach, six independent, uniformly distributed, random numbers are used to find emission origin $(\mathcal{R}_j^x, \mathcal{R}_j^y, \mathcal{R}_j^z)$, propagation direction $(\mathcal{R}_j^\theta, \mathcal{R}_j^\phi)$, and the wavenumber $(\mathcal{R}_j^\eta)$ for ray j. The random number relations for origin location and propagation direction can be found in [1], whereas the wavenumber selection scheme is discussed in [42]. When implemented on a finite volume computational mesh, the initial energy E^0 of each ray is obtained by relating the total energy content (E_i) and number of rays to be emitted (N_i) in each computational cell i by $E^0 = {}^{E_i}/_{N_i}$. Total number of rays in the entire simulation is then $N = \sum_i N_i$. In practice, however, the desired total number of rays N is prescribed and number of rays to be emitted from each cell is calculated based on the ratio of local emission from a given cell (i) and the total emission from the entire domain. This adaptive scheme ensures that the initial energy of all rays are within a narrow range making each ray almost equally important. It should

be noted here that number of rays emitted from one cell to another can be different and the actual total number of rays obtained this way is slightly (usually $< 1\%$) different than prescribed. This strategy has been discussed in details in [1]. Energy attenuation of rays during tracing can follow either a ballistic scheme (where a rays travels a randomly arbitrary distance determined by optical thickness of the medium and gets its energy is completely dumped only in the last computational cell) or an energy partitioning scheme [1]. In this work we follow the energy partitioning scheme. In this approach, energy from each ray is absorbed into the medium as it passes through each computational cell. After a ray containing energy E^0 and wavenumber η passes an optical distance τ_η inside a computational cell, its energy is attenuated to $E = E^0 e^{-\tau_\eta}$ as it dumps an amount of energy $\Delta E = E^0(1 - e^{-\tau_\eta})$ in to the local medium. The ray is traced until all its energy is attenuated completely (i.e., its energy becomes less than 0.1% of its original energy) or it moves outside the domain. The radiative source term for the medium is then determined as the difference between the energy gained from all rays passing through a computational cell and energy lost due to rays emitted from the cell.

With a sufficiently large number of rays, PMC methods can produce the exact solution regardless of the complexity of the problem. The accuracy of the PMC method is determined by either the actual error (from an 'exact' solution) of the mean solution or the standard deviation of an evaluated variable over multiple statistical iterations (*i.e.*, it's statistical error). The statistical error of a Monte Carlo simulation is represented by $O(N^{-0.5})$ where N refers to the number of rays sampled in the simulation.

3. Quasi-Monte Carlo method

The Monte Carlo methods rely on good random number generation schemes. In general, true random numbers can be generated by harvesting measurements related to some physical phenomena (*e.g.*, thermal noise, atmospheric noise, shot noise, etc.) using a dedicated hardware-based random number generator. However, for most computing purposes, where fast generation of random number is critical, users often resort to deterministic algorithm-based random numbers termed as *pseudorandom numbers*. The algorithms used to generate pseudorandom numbers are usually referred to as pseudorandom number generators (PRNGs). Since these pseudorandom numbers

are calculated using a deterministic algorithm, care needs to be taken so that the numbers generated from PRNGs show approximate characteristics of a true random distribution [43, 44]. It is desirable for pseudorandom numbers to have good unbiased distribution (*i.e.*, randomness), a long period (*i.e.*, the point at which the sequence starts to repeat), and repeatability [44]. The quality of "randomness" for a PRNG is, by design, dependent on the starting point or the pseudorandom sequence or 'seed.' For robustness often a physically-derived randomness (*e.g.*, thermal noise of a processor) is used to generate the seed. In most Unix-like systems a file `/dev/random` (or its variant) provides access to the noise collected from device driver and other sources [45] that can be used as a seed for a PRNG.

Quasi-Monte Carlo methods replace the PRNGs in favor of low-discrepancy sequences (LDS). An LDS distributes *quasi*-random samples in some *self-avoiding* fashion based upon a deterministic algorithm. The distribution of an LDS favors *uniformity* over *randomness*. Notably, the distribution of random samples will asymptotically reach uniformity with increase in number of samples. With equal subintervals, a PRNG produces outputs that have equal probability of an output landing in a given subinterval which can lead to clustering or gaps within the set. An LDS tries to eliminate these phenomena by generating points in a correlated manner, *i.e.*, filling the domain with *n-tuples* more quickly and evenly than PNRGs [46]. Low-discrepancy sequences can be identified visually by a set of points tending towards *equidistance* for any subset within the sequence; typically better spacing refers to lower discrepancy. For example, Fig. 1 shows the progression of distribution of random numbers obtained from a PRNG and a low-discrepancy sequence (Sobol sequence, in this case) for different sample sizes.

There are several LDS available in literature [47]. In this work, we use Sobol, Halton, and Niederreiter sequences based on recommendations from the literature [48, 49]. Sobol sequences are generated from a set of binary fractions called direction numbers [50]. Developing a Sobol sequence has been extensively discussed and the reader is recommended to the respective literature [*e.g.*, 48, 47, 51, etc.]. The efficient "gray code" algorithm by Antonov and Saleev is used this work to calculate multidimensional Sobol's sequence [48]. A Halton quasi-random number is generated by rewriting an integer j in base b, reversing the digits, and adding a preceding decimal point [52, 53]. The result is a fraction in base b. Niederreiter's quasi-random sequence based on

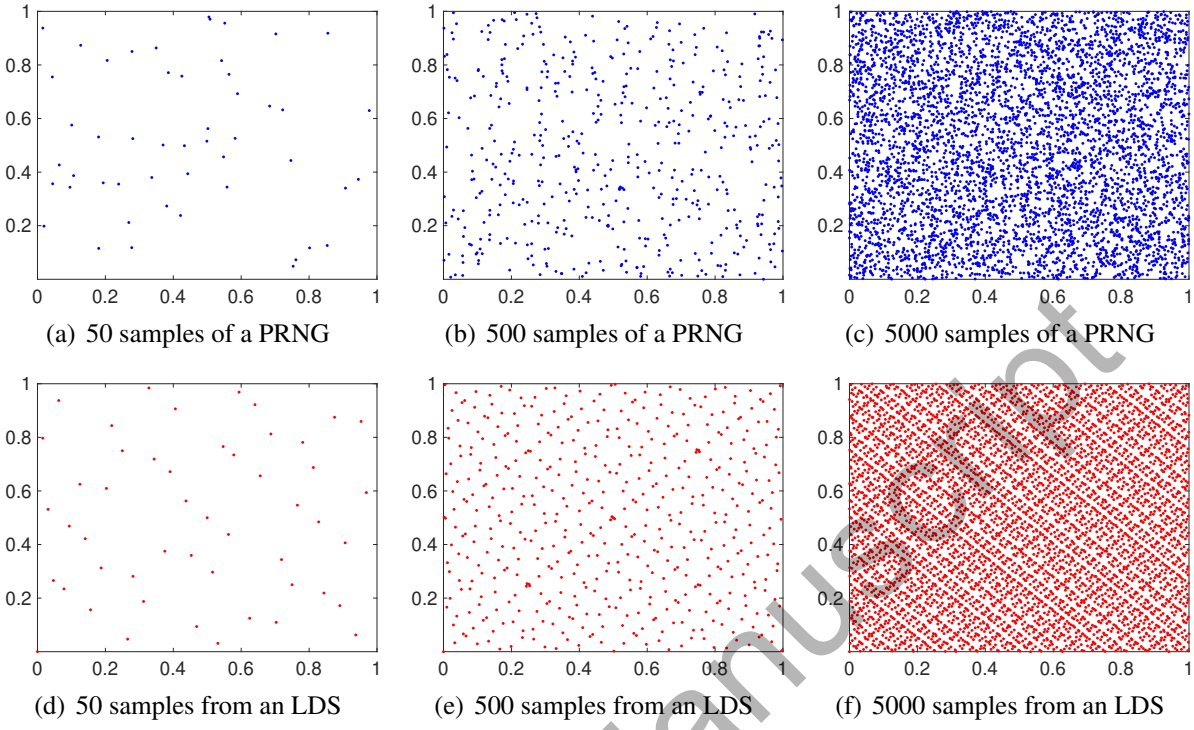

(a) 50 samples of a PRNG (b) 500 samples of a PRNG (c) 5000 samples of a PRNG

(d) 50 samples from an LDS (e) 500 samples from an LDS (f) 5000 samples from an LDS

Figure 1: Samples obtained in two-dimensional space from a PRNG and an LDS (Sobol)

the theory of *(t,s)*-nets in base b was introduced by Niederreiter [54, 55]. Sobol's sequence can be thought of as a generalized Niederreiter sequence in base 2. The calculation of Niederreiter's sequence is similar to Sobol's sequence with the exception of how direction numbers are generated. A more detailed review of these sequences can be found in [32, 47, 55].

As discussed earlier, PMC method requires emitting and tracing a statistically meaningful number of rays. The proposed quasi-Monte Carlo (QMC) method for thermal radiation does the same, but instead of use pseudorandom numbers to define each ray, quasi-random numbers from a six dimensional LDS is used. Therefore for ray j, the six random numbers corresponding to its emission origin $(\mathcal{R}_j^x, \mathcal{R}_j^y, \mathcal{R}_j^z)$, propagation direction $(\mathcal{R}_j^\theta, \mathcal{R}_j^\phi)$, and wavenumber $(\mathcal{R}_j^\eta)$, are substituted with $\mathcal{S}_j^1, \mathcal{S}_j^2, \ldots, \mathcal{S}_j^6$. Here $\mathcal{S}_j^n$ indicates j^{th} number in n^{th} dimension of the six-dimensional low-discrepancy sequence. Therefore, $\mathcal{S}_j^1, \mathcal{S}_j^2$ and $\mathcal{S}_j^3$ correspond to the emission origin, $\mathcal{S}_j^4, \mathcal{S}_j^5$ to the propagation direction, and $\mathcal{S}_j^6$ is for the wavenumbers.

4. Results and discussion

In this section we first present validation of the quasi-Monte Carlo (QMC) method for thermal radiation followed by a systematic performance comparison of the QMC and conventional Monte Carlo (MC) in multiple combustion-related configurations. The QMC scheme is validated against exact analytical solutions which are only available in simple configurations such as a one-dimensional plane-parallel media. Then we present three distinct, nongray combustion configurations followed by a discussion on the effect of emitting/reflective walls in the dimensionality of QMC. Finally the computational cost and efficiency of QMC is discussed.

As mentioned earlier, the accuracy of a Monte Carlo solver can be measured in terms of the actual error (ϵ) of the solution from the exact or benchmark solution or in terms of the standard deviation (σ) of the solution. The standard deviation and actual error for a good Monte Carlo simulation that uses unbiased and independent random samples follow each other. For example, there is a 95% probability that the actual statistical mean solution is within two standard deviations of the Monte Carlo mean. But if the random samples are not independent, this one-to-one relationship may not be true. Low-discrepancy sequence, by design provides equidistant samples, thereby is expected to reduce standard deviation compared to corresponding random samples [32]. In this work, we will evaluate the accuracy of the Monte Carlo and quasi-Monte Carlo methods in terms of actual error for two reasons. First, the actual error is a stronger indicator of accuracy. Second, QMC uses a deterministic sequence therefore different statistical runs will provide the same sequence making standard deviation an ambiguous measure for QMC. A short discussion on probabilistic bounds of standard deviation and error in QMC is presented in Appendix A.

Since this implementation is based on a finite volume framework, the local root-mean-square (RMS) relative error is defined at each computational finite volume cell (index i) as

$$\epsilon_i = \left[\frac{1}{S} \sum_{s=1}^{S} \left(\frac{q_i^s}{q_i^o} - 1 \right)^2 \right]^{1/2}, \tag{2}$$

where q refers to the target variable for solution, S refers to the number of statistical runs, q_i^s is the solution from the Monte Carlo simulation, and q_i^o is the solution from the analytical or benchmark

solution. All configurations with the MC method use $S = 10$ statistical runs, whereas QMC is run only once. The target variable for accuracy estimation in this work is either local radiative heat source (*i.e.*, divergence of local radiative heat flux, $\nabla \cdot Q$ [W/m^3]), local radiative absorption per unit volume (Q_{abs} [W/m^3]), or wall heat flux (Q''_{wall} [W/m^2]) as appropriate for each test configuration. Additionally, as done in [56], comparison of "efficiency" of Monte Carlo schemes are done via a "figure of merit" (FoM) which also takes into account computational time. In this work, FoM is calculated based on spatially-averaged RMS relative error ($\bar{\epsilon}$)

$$\text{FoM} = \frac{1}{\bar{\epsilon}^2 t}, \tag{3}$$

where t is the simulation time. A high FoM score is indicative of a good Monte Carlo simulation *i.e.*, low error at low computational cost.

4.1. Validation in one-dimensional plane-parallel media

The configuration used for validation is a one-dimensional gas slab bound by two parallel, black walls separated by 0.1 m. Several combinations of temperature and absorption coefficient profiles were tested for validation and only three representative cases are presented for brevity. These cases are listed in Table 1. The gray participating media was defined by imposing a specific profile of Planck-mean absorption coefficient (κ_P). The nongray medium consisted of 20% (by mole) CO_2 and rest of the medium was radiatively non-participating. A line-by-line (LBL) database obtained from HITEMP spectroscopic database [57] was used to evaluate then nongray radiative properties of CO_2.

Table 1: One-dimensional validation cases. In case (2) the x [m] is the distance from one wall.

Case	(1)	(2)	(3)
Abs. Coeff.	gray, $\kappa_P = 1$ m^{-1}	gray, $\kappa_P(x) = 1 + 750x$ m^{-1}	nongray LBL
T_{medium}	1200 K	$T(x) = 1700 - 5000x$ K	2000 K
Walls	800 K, black	800 K, black	cold, black

The results for the three cases are shown in Figs. 2–4. Figures 2(a), 3(a), and 4(a) show the comparison of $\nabla \cdot Q$ calculated from the MC and QMC with three different LDS (Sobol, Halton, and

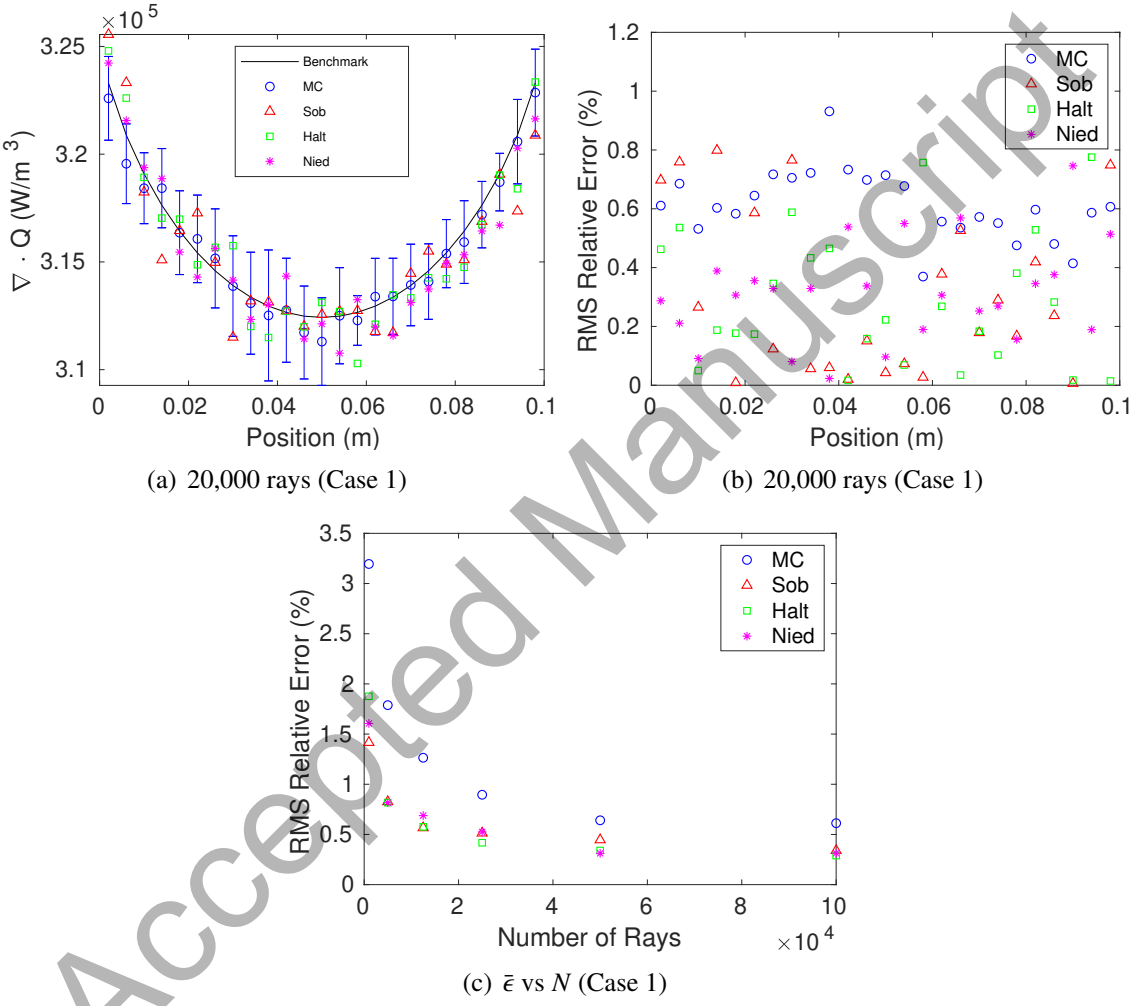

(a) 20,000 rays (Case 1)

(b) 20,000 rays (Case 1)

(c) $\bar{\epsilon}$ vs N (Case 1)

Figure 2: Accuracy and convergence of MC and QMC using Sobol, Halton, and Niederreiter sequences in Case 1

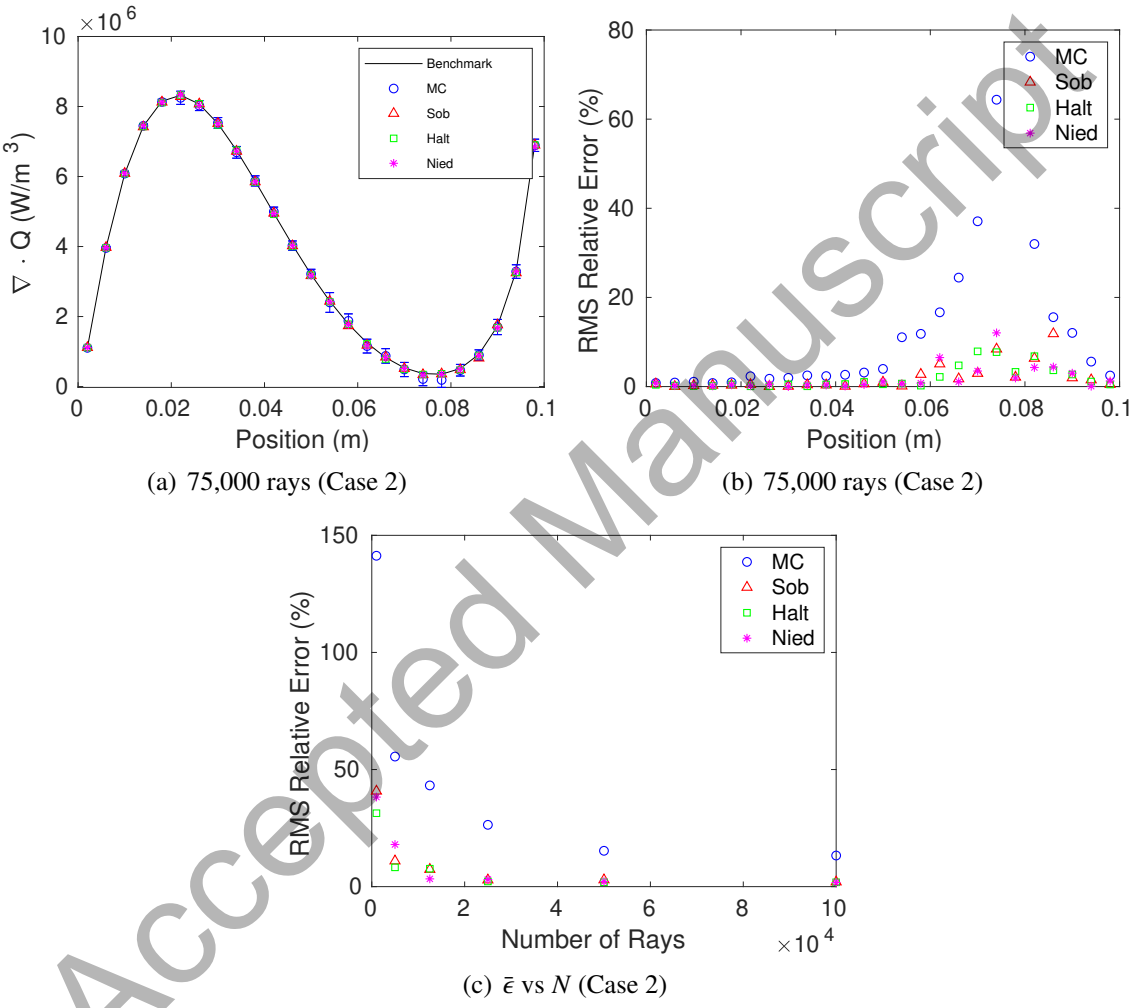

(a) 75,000 rays (Case 2)

(b) 75,000 rays (Case 2)

(c) $\bar{\epsilon}$ vs N (Case 2)

Figure 3: Accuracy and convergence of MC and QMC using Sobol, Halton, and Niederreiter sequences in Case 2

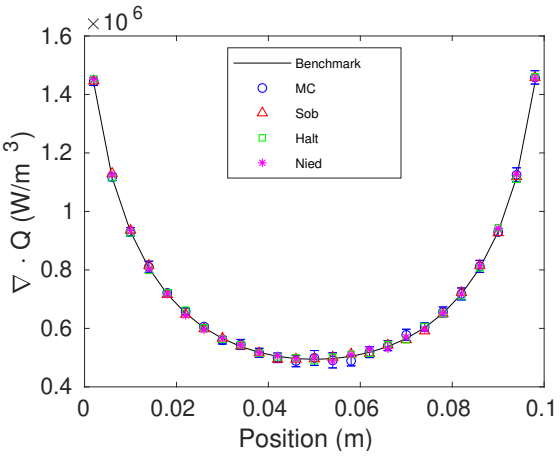

(a) 100,000 rays (Case 3)

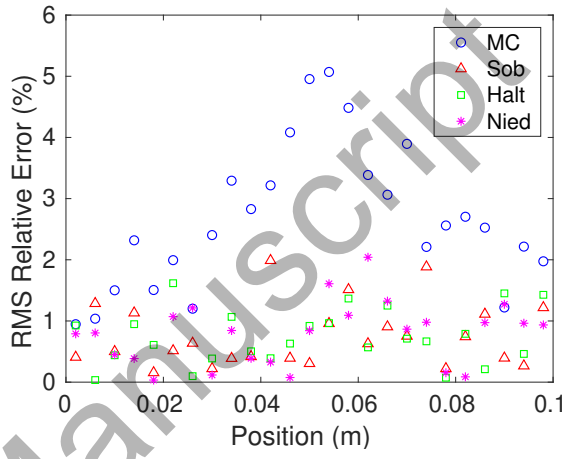

(b) 100,000 rays (Case 3)

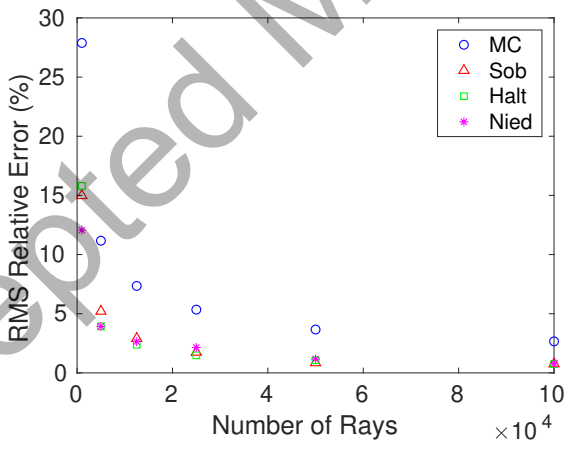

(c) $\bar{\epsilon}$ vs N (Case 3)

Figure 4: Accuracy and convergence of MC and QMC using Sobol, Halton, and Niederreiter sequences in Case 3

Niederreiter), along with the analytical solution [1]. Both MC and QMC show good agreement with the analytical solution in all cases. The variations in local RMS error (ϵ_i) can be seen in Figs. 2(b), 3(b), and 4(b). In all three cases, local errors from QMC are generally lower than that from MC. Finally, Figs. 2(c), 3(c), and 4(c) show the "convergence rate" of QMC and MC. The convergence rate is defined as how fast the average relative RMS error ($\bar{\epsilon}$) decrease with increase in the number of rays. It can be seen from Figs. 2(c), 3(c), and 4(c) that QMC converges quicker than MC. A further discussion on convergence rate can be found in Appendix A. It is also evident that all three low-discrepancy sequences produce same levels of error and neither shows any advantage over another.

4.2. Three-dimensional combustion simulations

The three combustion configurations chosen in this study are a high-pressure gas turbine, a constant-volume spray combustion chamber, and a turbulent pool fire. The choice of these cases are to include a diverse set of configurations as possibly encountered in combustion simulations. The first two configurations involve hot emitting walls, whereas the third one involves open boundaries. The second and third configurations include nongray soot along with nongray gases. Additionally, the first two configurations are based on a Reynolds-averaged simulation (RAS) whereas the third one is based on a large eddy simulation (LES). In all simulations CO_2, H_2O, CO, and soot (when present) are used as participating media. The spectral properties of gases are modeled by line-by-line (LBL) databases constructed from HITEMP spectroscopic data [57].

An analytical solution is impossible to obtain for these configurations. Therefore, solutions calculated from a significantly large number of rays (the actual number varies from one configuration to another as discussed later) with 50 statistical iterations of a MC simulation are treated as the benchmark solutions for the purpose of evaluating RMS error as shown in Eqn. 2. Furthermore, local error is calculated in terms of volumetric absorption in these cases. This choice is made because of the presence of locally strong optically thick regions, which lead to a near-zero value of $\nabla \cdot Q$ in some locations. Therefore calculation of relative error based on $\nabla \cdot Q$ can be misleading. Moreover, local emission can be determined analytically and the uncertainty of the

radiative transfer in MC/QMC essentially comes from the randomness in resolving the absorption term.

4.2.1. A high-pressure gas turbine

The first three-dimensional configuration is based on the SGT-100 industrial gas turbine combustor with an output of approximately 5 MW and pressure ratio of approximately 15:1 [58]. Snapshots of the scalar fields are taken from a numerical simulation done by Ren et al [59]. The simulations were performed in a Reynolds averaged simulation (RAS) framework with standard k-ϵ turbulent model and GRI-Mech 2.11 chemical mechanism [see 59, for details]. The computational domain is shown in Fig. 5, and the scalar fields of the snapshot used in this study are shown in Fig. 6. The gas turbine, referred to as the GT configuration, has 15,718 finite volume cells for the three-dimensional wedge domain as shown in Fig. 5. The walls are considered black and emitting at a temperature 673 K. As before, CO_2, CO, and H_2O are treated as participating media.

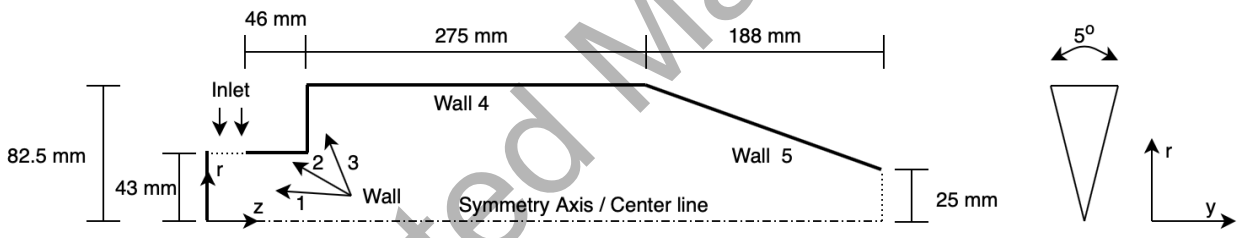

Figure 5: GT configuration

The benchmark solution for the GT case was run with 10^7 rays and 50 statistical Monte Carlo simulations. For accuracy comparison, both MC and QMC was run with 1.6×10^6 rays. We performed $S = 10$ statistical simulations of MC to obtain statistical mean and RMS error. The actual scalar field for radiative source term and absorption are indistinguishable between benchmark, MC, and QMC runs and hence are not shown here. Instead, we show one axial (at $r = 0.03$ m) and one radial (at $z = 0.1$ m) profile of the absorption as marked in Fig. 6. Figure 7 shows the local radiative absorption along these lines. Both the MC and QMC methods are in very good agreement with the benchmark solution and the results from QMC fall within the error bars of the MC method throughout. As in the case of one-dimensional configuration, QMC converges faster

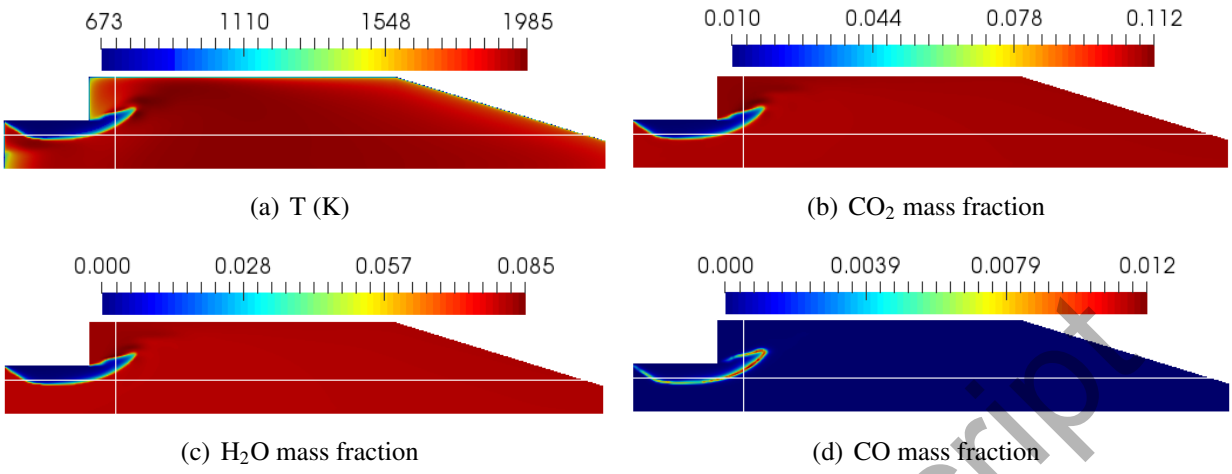

(a) T (K) (b) CO_2 mass fraction

(c) H_2O mass fraction (d) CO mass fraction

Figure 6: Scalar field contours for GT configuration

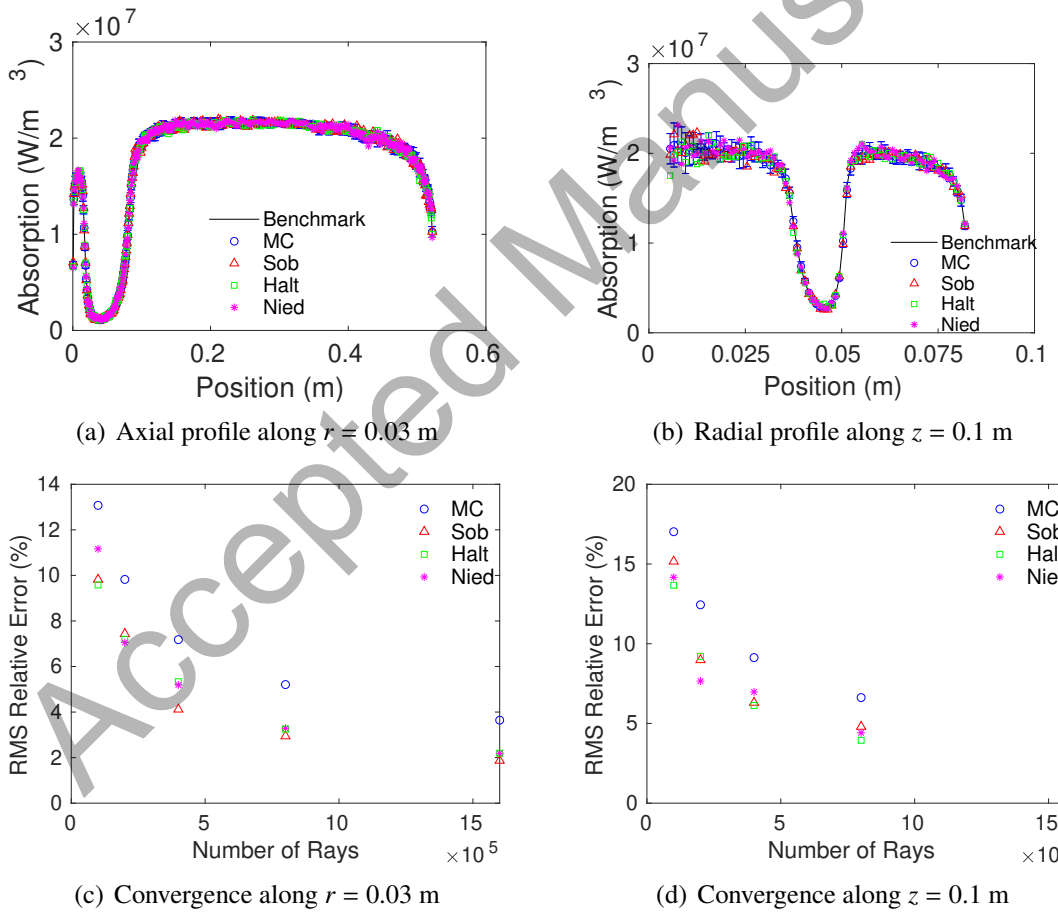

(a) Axial profile along $r = 0.03$ m (b) Radial profile along $z = 0.1$ m

(c) Convergence along $r = 0.03$ m (d) Convergence along $z = 0.1$ m

Figure 7: Profiles of radiative absorption from MC and QMC with different LDS (with 1,600,000 rays) along two lines (see Fig. 6) in GT configuration

than MC with increase in number of rays (further discussion in Appendix A). It can be seen that the error of MC and QMC from the benchmark solution is higher near the centerline. It is because the volume of computational cells near the centerline is much smaller and radiation being a volumetric phenomena, the number of rays passing through a cell is also proportional to its volume. Therefore, smaller cells near centerline lead to slightly degraded statistics in MC/QMC.

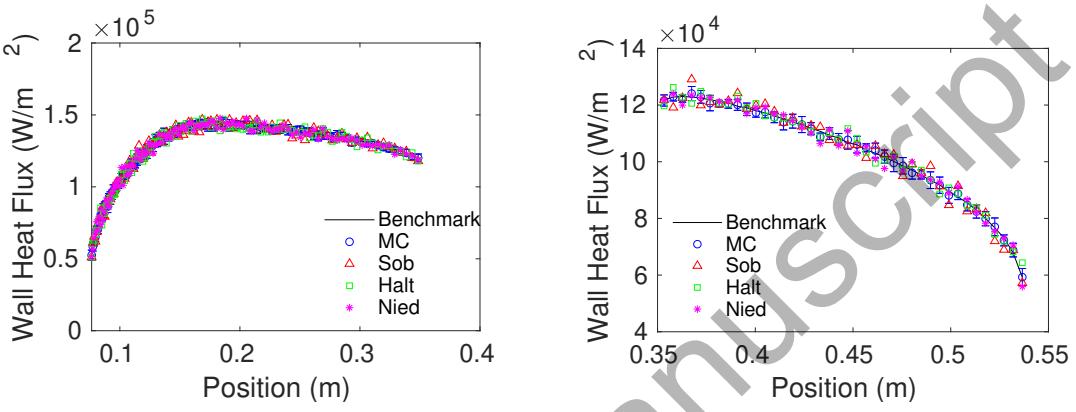

(a) Wall 4 (b) Wall 5

Figure 8: Wall heat flux profiles from MC and QMC with different LDS (with 1,600,000 rays) along two walls (see Fig. 5) in GT configuration

The GT configuration has five walls around the combustion domain. Radiative heat loss to walls is an important quantity. Figure 8 shows the wall heat flux of the benchmark, MC, and QMC simulations along walls 4 and 5 shown in Fig. 5. It is interesting to see that although the absorption in the media is predicted well by QMC, the wall heat flux from QMC shows larger error than MC at some locations. However, the average relative error (not shown) in wall heat flux from QMC still remains lower than MC, albeit with a more scattered pattern (*i.e.*, a larger range) in error distribution in QMC. Another point of note that as seen in Sec. 4.1, there is no noticeable difference between the three low-discrepancy sequences. Therefore, for clarity, we will use only Sobol's sequence for the rest of the study.

4.2.2. Constant-volume spray combustion chamber (Spray-A)

The second case considered is from the Engine Combustion Network's (ECN) Spray-A configuration [see 60, for details]. This configuration, referred to as Spray-A, is a constant-volume combustion chamber where liquid n-dodecane is injected as high-pressure spray. The snapshot is

taken from the RAS results presented in [61, 62] at a time when all spray has evaporated. The computational configuration is a three-dimensional wedge mesh with 12,800 finite volume computational cells as shown in Fig. 9. The walls are hot at 850 K and emits as black surfaces. The peak soot volume fraction in the domain is 7.7 ppm. Along with the LBL data for the participating gases (CO_2, CO, and H_2O) soot is also treated as participating media. Radiative properties of soot is modeled based on a wavelength-dependent correlation [63]. Nature of radiative properties of soot is much closer to black body than the gases, hence we chose a case where there is a significant amount soot. The scalar fields of this case are shown in Fig. 10.

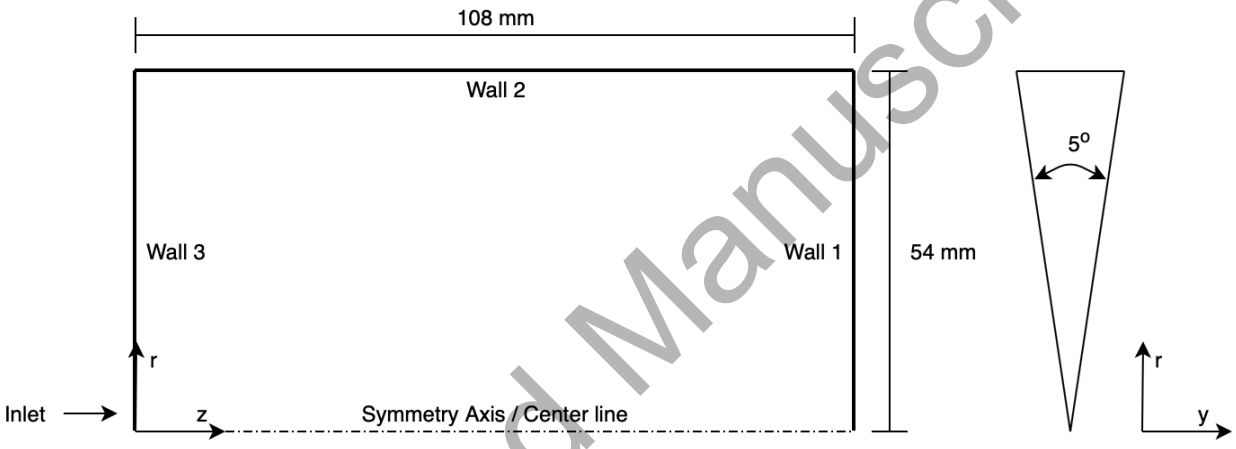

Figure 9: Spray-A configuration geometry

The benchmark solution for this case was based on 50 statistical runs of conventional MC with 10^7 rays. The MC and QMC runs for performance comparison were done using 1.6×10^6 rays. As before, $S = 10$ statistical runs were used for MC and only one deterministic run for QMC. Similar to GT case, we present profiles of radiative absorption along two lines for better clarity. Radiative absorption is compared in Fig. 11 along the axial $r = 0.004$ m, and radial $z = 0.105$ m lines marked in Fig. 10. Both QMC and MC show good agreement with the benchmark solution and the QMC method is within one standard deviation throughout the lines. As before larger error can be observed near the centerline.

Figure 12 shows the wall heat flux results from MC and QMC. While the results at the Wall 1 matches well with the benchmark solution, the Wall 2 results vary wildly. In fact, along Wall 2 not only the standard deviation from the MC is quite large, but also at several locations the QMC

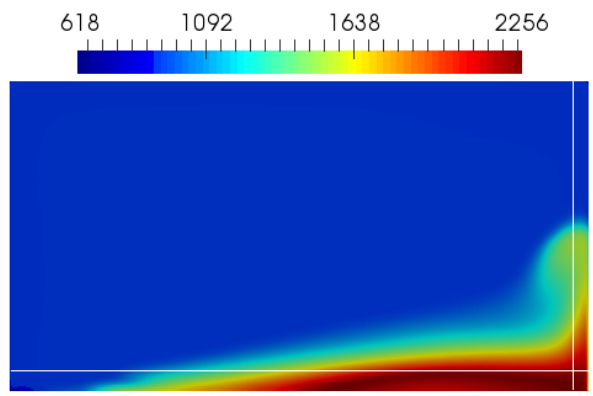

(a) T (K)

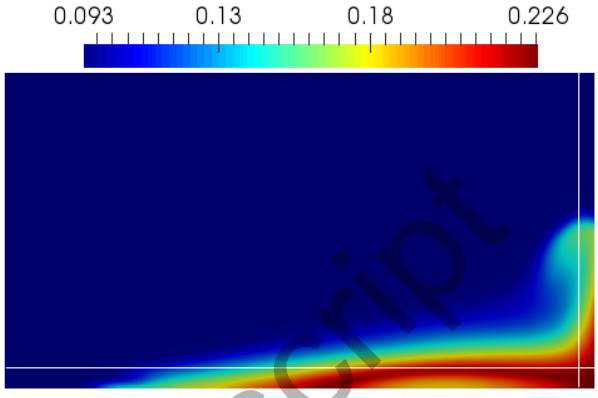

(b) CO_2 mass fraction

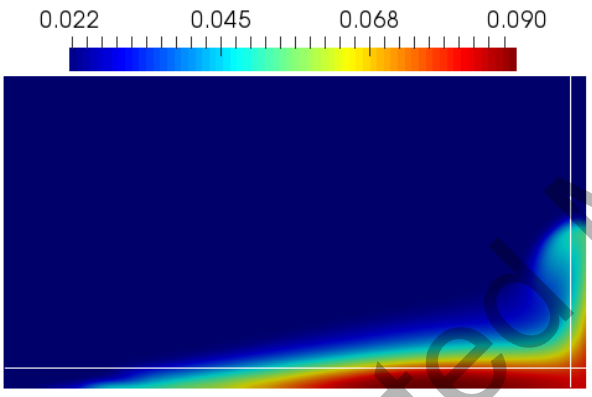

(c) H_2O mass fraction

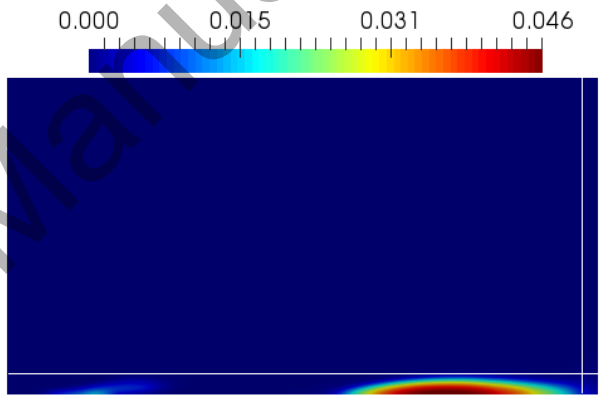

(d) CO mass fraction

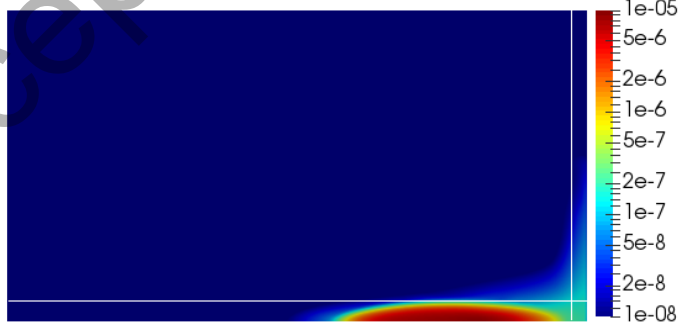

(e) Soot volume fraction

Figure 10: Scalar field contours for Spray-A configuration

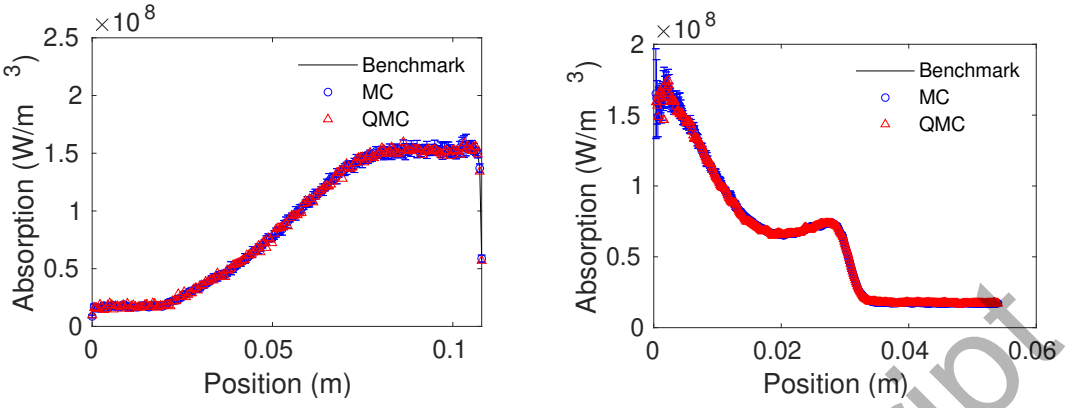

(a) Axial profile along $x = 0.004$ m (b) Radial profile along $z = 0.105$ m

Figure 11: Profiles of radiative absorption from MC and QMC (with 1,600,000 rays) along two lines (see Fig. 10) in Spray-A configuration

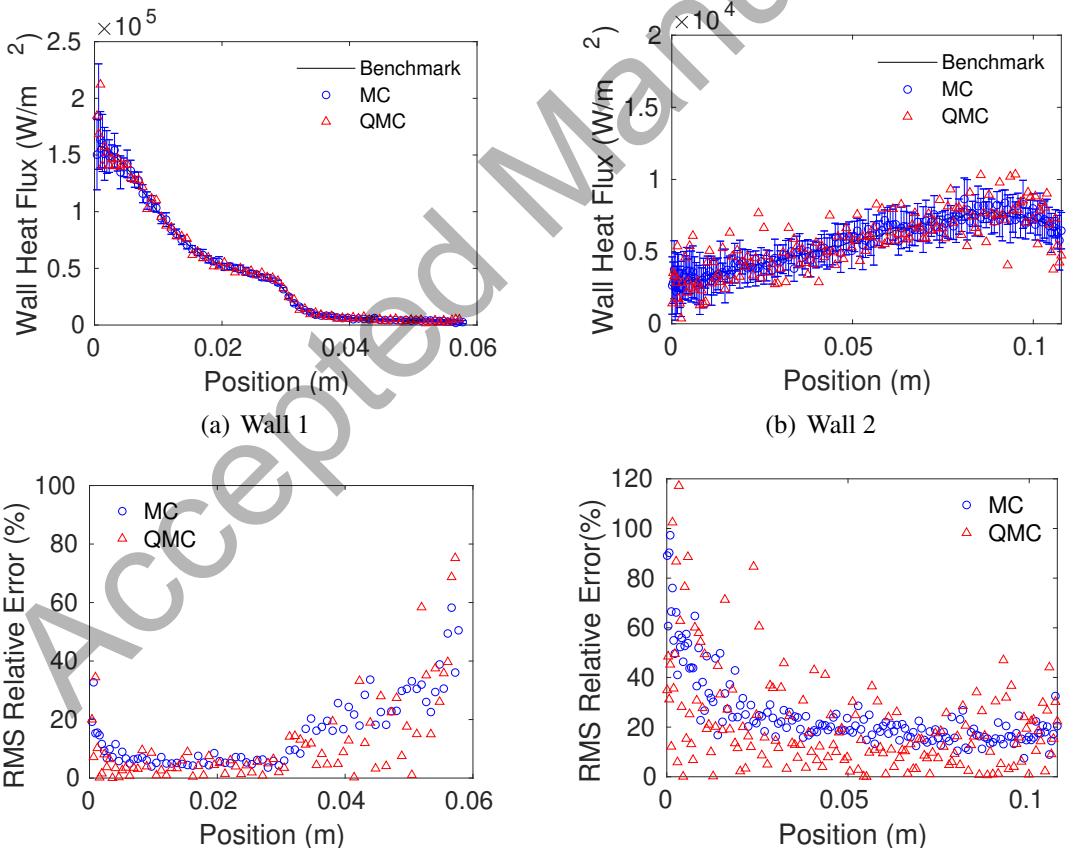

(a) Wall 1 (b) Wall 2

(c) Wall 1 RMS relative error (d) Wall 2 RMS relative error

Figure 12: Wall heat flux profiles from MC and QMC (with 1,600,000 rays) along two walls (see Fig. 9) in Spray-A configuration

results lie beyond one standard deviation from the MC. A point of note here is that the actual value of wall heat flux at Wall 2 is considerably smaller than Wall 1. The comparison of relative error in Fig. 12(c) and 12(d) indicate that both QMC and MC predict the solution well in regions of higher wall flux (Fig. 12(c) $r = 0$ to 0.03 m) and the statistics degrades where the heat flux is small. A factor contributing to higher relative error in lower heat flux regions is the fact that for computational efficiency, the number of rays emitted from a location is proportional to the energy content of the location (importance sampling) [1]. Since the region near Wall 2 is comparatively cooler than the core regions (Fig. 6), the total number of rays in the region near Wall 2 is less than other parts (*e.g.*, near the flame). This leads to higher statistical error near Wall 2.

4.2.3. A laboratory-scale turbulent pool fire

The final case is an n-heptane turbulent pool fire experimentally studied by Klassen and Gore [64]. The diameter of the pool is 7.1 cm and measured flame height is 34.5 cm. The radiant fraction of this case is approximately 29%. The pool fire was simulated using a large eddy simulation (LES) approach with detailed chemistry and a semi-empirical soot model [see 65, 66, for further details]. The snapshot used in this study is scaled from a snapshot of the flame reported in [65, 66]. The computational mesh, shown in Fig. 13, contains roughly 400,000 cells with a radius of 0.4 m and height of 0.6 m. All boundaries except the bottom pool surface are open boundaries. The ambient temperature and pressure are 300 K and 1 atm, respectively. The temperature at the fuel inlet is constant at 371.6 K (the boiling point of n-heptane).

Figure 14 shows contours of instantaneous flame structure and Fig. 15 shows contours of radiative absorption and errors along a vertical plane. The benchmark solution, shown in Fig. 15(a), was obtained using 10^8 rays with 50 statistical analyses of MC. Contours of volumetric absorption for MC and QMC with 4×10^7 rays are shown in Figs. 15(b) and 15(c). As before, $S = 10$ statistical runs of MC was conducted to evaluate mean values shown in Fig. 15(b). Figures 15(d) and 15(e) show the absolute error for MC and QMC throughout the computational domain when compared with the benchmark solution. Radiative absorption with QMC is shown to have better agreement with the benchmark solution throughout the computational domain, albeit with a few locally high-

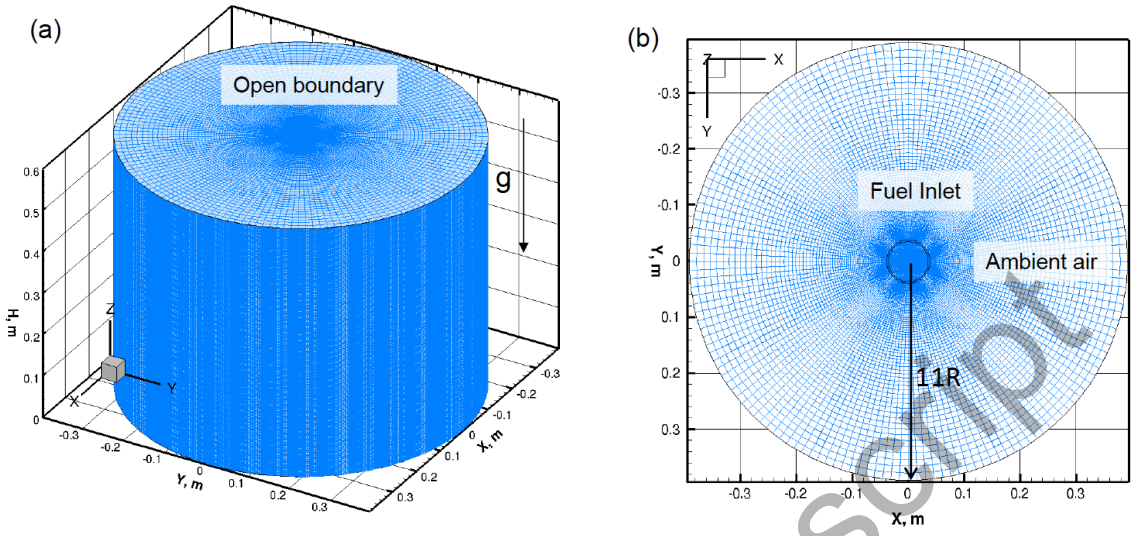

(a) Computational domain (b) Pool surface

Figure 13: Computational geometry for the pool fire case

error locations. Profiles of radiative absorption along a line shows similar trends as seen in other cases and are not shown here for brevity.

4.3. *Effect of emitting/reflecting walls on the dimensionality of QMC*

The presence of emitting/reflecting walls changes the dimensionality of Monte Carlo solution. The wall faces are planar faces. Therefore one needs only two, instead of three, parameters to characterize origin of wall-emitted rays (say, $\mathcal{R}_j^x, \mathcal{R}_j^y$ for MC and $\mathcal{S}_j^1, \mathcal{S}_j^2$ for QMC). In the context of QMC, since only five numbers from a six-dimensional sequence are utilized in some rays, there is an expected global loss of "uniformity" within the sequence. However, the effect of this loss of uniformity is likely negligible, for two reasons. First, usually energy content, and hence number of rays emitted from walls are much less compared to the combustion medium. For example, in the GT simulations more than 1.5×10^6 rays were emitted from the participating medium (*i.e.*, internal cells) while approximately 2.5×10^4 rays were emitted from walls. Second, any subset of an LDS will also tend to be an LDS by design. Therefore, overall loss of uniformity is expected to be small because of this dimensional discrepancy between wall-emitted and medium-emitted rays.

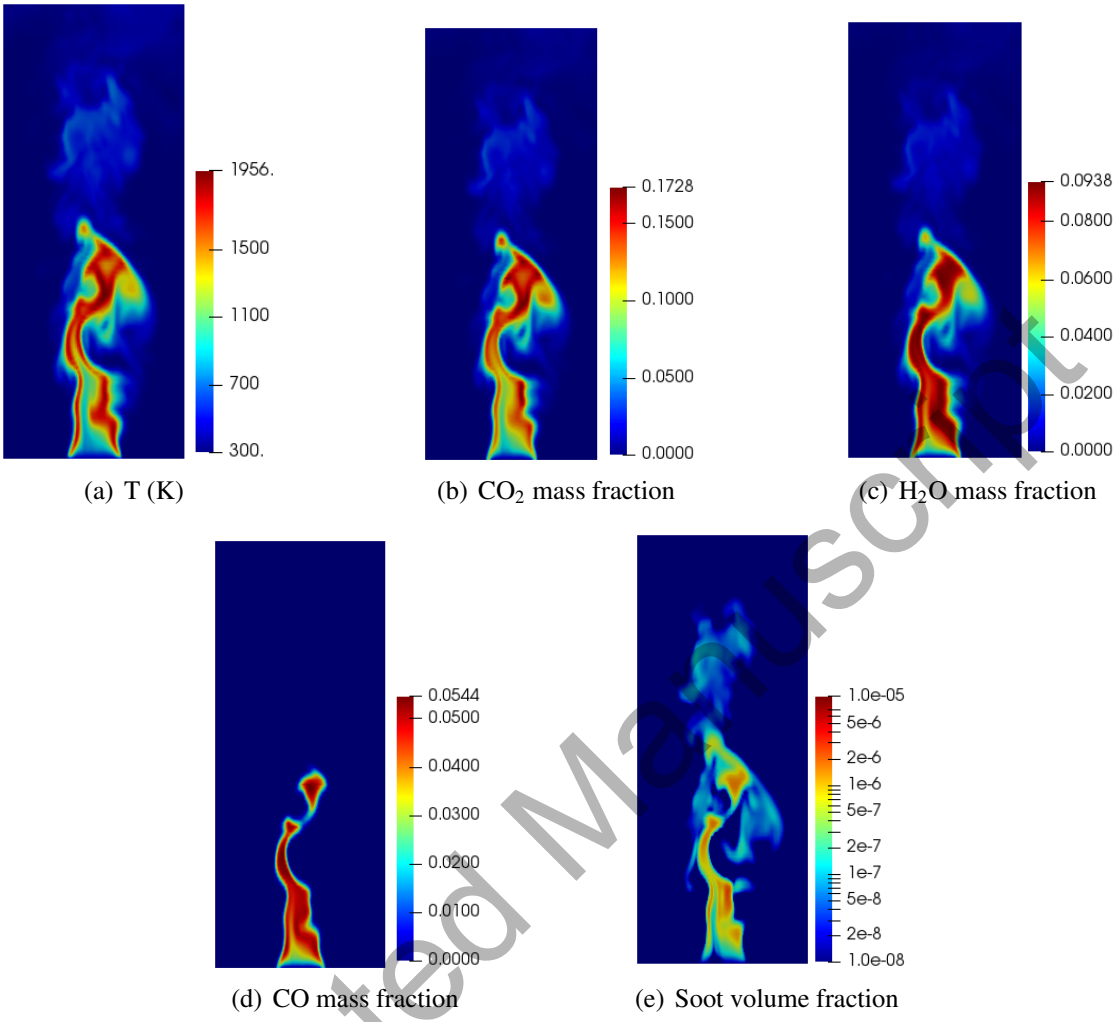

(a) T (K) (b) CO_2 mass fraction (c) H_2O mass fraction

(d) CO mass fraction (e) Soot volume fraction

Figure 14: Contours of the scalar fields along a vertical plane of the pool fire.

Reflective walls, on the other hand, poses a more severe loss of dimensionality. Diffuse reflection requires generation of two new random numbers for determining the direction of the reflected ray every time a reflection event occurs. If one chooses to use the same six-dimensional LDS for reflection events (*i.e.*, only uses $\mathcal{S}_j^4$ and $\mathcal{S}_j^5$ and discards all others), a large number of reflection events could considerably affect the uniformity of a the sequence and degrade the statistics of the simulation. This phenomenon is shown in Fig. 16. Here we modified the GT case discussed earlier and made the walls 50% reflective keeping everything else same as before. Using the same original six-dimensional Sobol sequence the results from QMC shows noticeable under-prediction of absorption. In this case, as before, 1,600,000 rays were used in MC and QMC simulations.

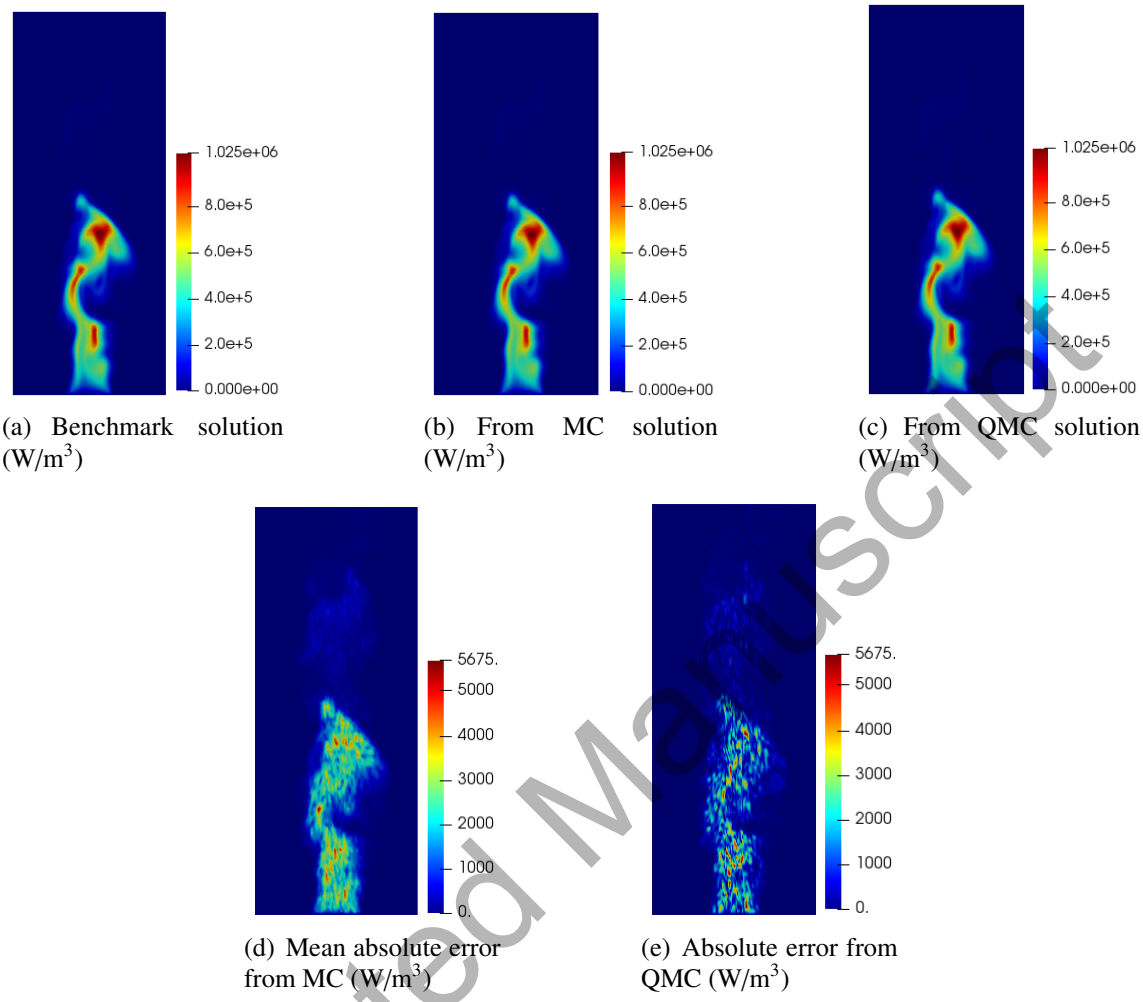

(a) Benchmark solution (W/m^3)

(b) From MC solution (W/m^3)

(c) From QMC solution (W/m^3)

(d) Mean absolute error from MC (W/m^3)

(e) Absolute error from QMC (W/m^3)

Figure 15: Contours of radiative absorption and absolute error in radiative absorption calculations along a vertical plane in the pool fire case. Both MC and QMC were run with with 4×10^7 rays.

And total reflection events in this case was found to be approximately 1,200,000. This means that approximately a total of 2,800,000 sets from a single Sobol sequence were sampled, but in 40% of times only $\mathcal{S}_j^4$ and $\mathcal{S}_j^5$ were utilized discarding other dimensions. This increases discrepancy in the simulation.

Therefore, it is proposed that two independent low-discrepancy sequences are used to accommodate simulations where reflection is present. The first sequence is the six-dimensional as before, and a second two-dimensional sequence is used only to determine the direction of reflected rays in reflection events. For example, $\mathcal{S}_j^1, \mathcal{S}_j^2, \ldots, \mathcal{S}_j^6$ would be used initially to emit j^{th} ray, then a

separate, independent two-dimensional sequence $\mathcal{S}'^1_k, \mathcal{S}'^2_k$ would handle the k^{th} reflection event. Here $\mathcal{S}'$ indicates a two-dimensional Sobol sequence independent of the original six-dimensional $\mathcal{S}$. The results from the two independent sequences improves greatly as seen in Fig. 17. While it is not shown here, in a similar way, two independent sequences can be used in QMC to tackle scattering events as well.

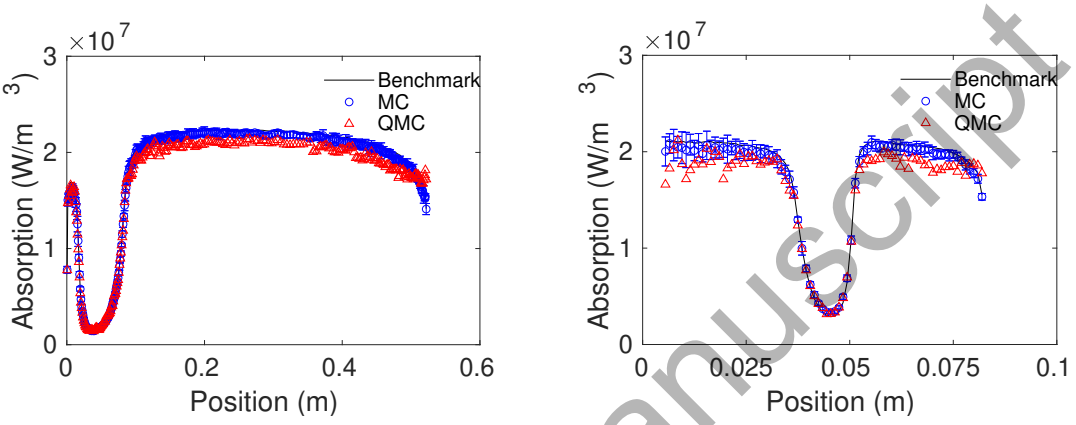

(a) Along $r = 0.03$ m (b) Along $z = 0.1$ m

Figure 16: Radiative absorption profiles for GT with reflective walls from MC and QMC with single six-dimensional Sobol sequence

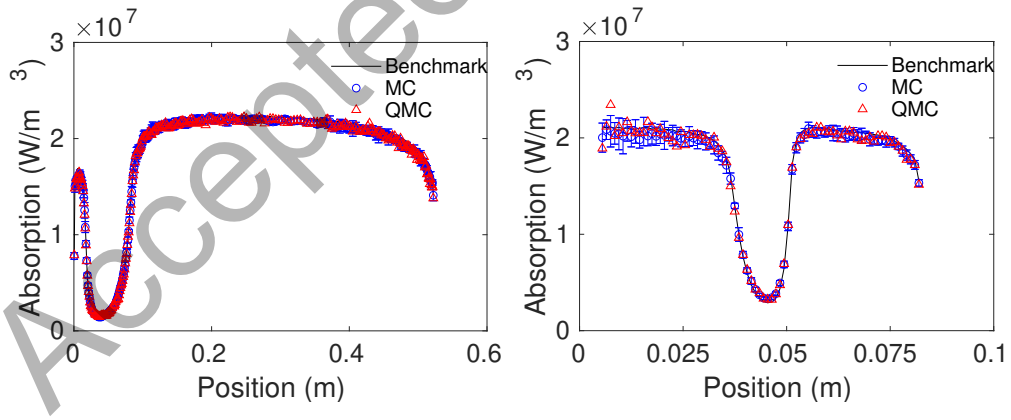

(a) Along $r = 0.03$ m (b) Along $z = 0.1$ m

Figure 17: Radiative absorption profiles for GT with reflective walls from MC and QMC with two independent Sobol sequences

4.4. Computational efficiency and Figure of Merit

Typically in a Monte Carlo solver for thermal radiation most of the computational effort is spent in tracing the rays as tracing requires an exhaustive face-line intersection search at every computational cell each ray goes through. Whereas the generation of random numbers and the estimation of origin, direction, and wavenumber of a ray is needed to be done only once in a ray's lifetime. Re-generation of random numbers for a ray is required only when a reflection or a scattering event is encountered. The base Monte Carlo code used in this study spends roughly 90% time in tracing and only 10% in generation of random numbers and calculation of origin, direction, and wavenumber of the rays. The computational overhead of Sobol sequence is very similar to that of PRNG algorithm used in the MC simulations in this study [67]. However, the total computational effort of $S = 10$ MC simulations is slightly higher than ten times the corresponding QMC run with same number of rays as shown in Table 2, possibly due to the different overheads.

Table 2: Computational cost of QMC and PMC in 3D cases. Each simulation was performed on a single Intel Xeon `E5-2687Wv4` processor.

Case	No. of cells	No. of rays per run	Computational cost (s)	
			QMC	MC
			one run	10 runs
GT	15,718	1.6×10^6	32.2	429
Spray-A	12,800	1.6×10^6	18.6	275
Pool Fire	392,000	4.0×10^7	4,853	48,751

The advantage of QMC is further amplified when the computational cost is considered along with the statistical accuracy of the simulation by using a Figure of Merit (FOM). The FoM metric as shown in Eqn. 3 gives an idea of this cost-accuracy benefit of QMC. Figure 18 shows the FoM based on average RMS relative error along the two lines for each combustion simulation (GT and Spray A). Since there were 10 statistical simulations of MC as opposed to one deterministic simulation of QMC, the computational run time is expected to be approximately 10 times more for the MC. This would indicate a factor of $S = 10$ increase in FoM for QMC over MC. However, it should be noted here that the in a MC simulation error reduces with the square-root of the number of samples, whereas computational cost increases almost linearly. Therefore, the FoM of a MC simulation is expected to vary only slightly with the change in number of rays (N) or statistical

runs (S). Nevertheless, Fig. 18 shows that in all three cases the increase in FoM due to QMC is more than a factor of $S = 10$ and somewhere closer to a factor of 30 to 50. This indicates that QMC not only provides a way to eliminate several statistical runs required for MC, but it can produce a lower statistical error than a single MC simulation. Similar results can be seen in Fig. 19, where
385 the FoM is calculated based on the wall heat flux for both the GT and Spray-A configurations. As seen in the wall heat flux comparisons (Figs. 8 and 12, the error margin for QMC is larger in terms of wall heat flux. This is reflected in reduction of relative advantage in the FoM plots in Fig. 19. Nevertheless, even with higher variation in error for the wall heat flux, the FoM of QMC is more than an order of magnitude higher than that of MC.

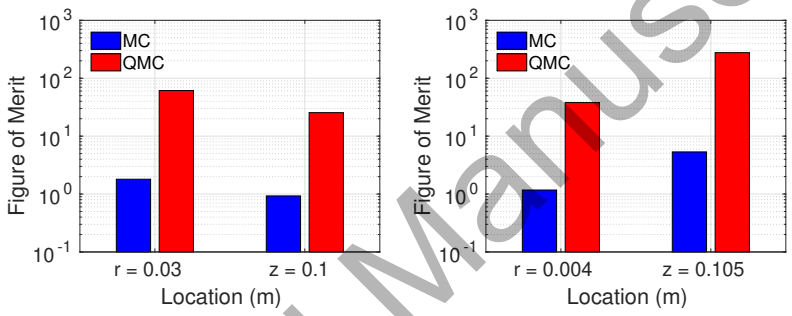

(a) GT with 1,600,000 rays (b) Spray-A with 1,600,000 rays

Figure 18: Figure of Merit (FoM) along two different lines of MC and QMC simulations for GT and Spray-A configurations

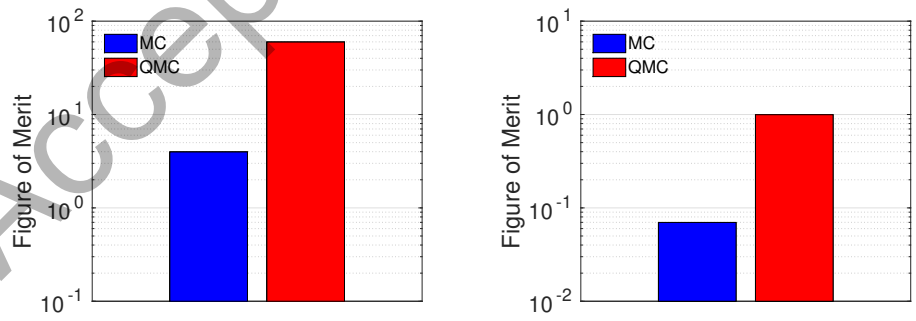

(a) GT with 1,600,000 rays (b) Spray-A with 1,600,000 rays

Figure 19: Figure of Merit (FoM) for both walls (see Fig. 8 and 12) in the GT and Spray-A configurations in MC and QMC simulations.

5. Conclusion

Monte Carlo ray tracing schemes for radiative heat transfer are the most accurate and robust solvers for thermal radiation but the high computational costs make them impractical for large scale simulations. The Quasi-Monte Carlo (QMC) method presented in this work addresses this bottleneck by replacing the random number sampling mechanism in traditional MC methods with a low-discrepancy sequence (LDS). A systematic performance comparison was done with both MC and QMC methods. First, the QMC method was validated in several one-dimensional configurations where it was shown that QMC has better accuracy at lower costs compared to MC. Then, QMC was extended to relevant three-dimensional combustion simulations. In terms of local and averaged RMS relative error, the QMC had lower error in these simulations as well. Three LDS – Sobol, Halton, and Niederrieter sequences – were used in the QMC and it was found that all three sequences produce same quality results. It was advantageous to define a figure of merit (FoM) to show the coupled nature of accuracy and computational costs for QMC, where a high FoM was indicative a good Monte Carlo simulation. For any given simulation the FoM for QMC was greater than MC. Because QMC required just one simulation, while MC algorithm used here (as proposed in [1]) requires a statistically significant number (S) of simulations (here, $S = 10$), the computational costs of QMC is reduced S-fold. In practice the gain in FoM was found to be *greater* than S-fold due to reduced error from QMC. Although the current study was done using frozen-field configurations, the similar advantage is expected to hold true for QMC in coupled simulations by restarting the LDS every timestep whenever the RTE solver is invoked. In conclusion, QMC is an attractive alternative to traditional MC methods for radiative heat transfer calculations due to its computational cost and accuracy advantages.

Acknowledgement

This material is based upon work supported by the National Science Foundation (NSF) under Grant No. 1756005. The authors would also like to thank Dr. Tao Ren for providing the snapshot for GT case, Mr. Khaled Mosharraf Mukut for providing the Spray-A case, and Ms. Bifen Wu & Dr. Xinyu Zhao for providing the base snapshot for the pool fire case.

References

[1] M. F. Modest, Radiative Heat Transfer, Academic Press, 2013.

[2] J. R. Howell, M. P. Mengüc, R. Siegel, Thermal Radiation Heat Transfer, 6th Edition, CRC Press, Boca Raton, FL, USA., 2015.

[3] J. C. Chai, H. S. Lee, S. V. Patankar, Ray effect and false scattering in discrete ordinate method, Numerical Heat Transfer , Part B : Fundamentals 24 (1993) 373–389.

[4] B. Hunter, Z. Guo, Numerical smearing, ray effect, and angular false scattering in radiation transfer computation, International Journal of Heat and Mass Transfer 81 (2015) 63–74.

[5] S. P. Roy, J. Cai, W. Ge, M. Modest, Computational cost and accuracy comparison of radiation solvers with emphasis on combustion simulations, in: Proceddings of CHT-15 ICHMT International Symposium on Advances in Computational Heat Transfer, Piscataway, NJ, 2015.

[6] T. Smith, Z. Shen, J. Friedman, Evaluation of coefficients for the weighted sum of gray gases model, Journal of Heat Transfer 104 (1982) 602–608.

[7] F. Cassol, R. Brittes, c. Fran O. F. Ezekoye, Application of the weighted-sum-of-gray-gases model for media composed of arbitrary concentrations of H_2O, CO_2 and soot, International Journal of Heat and Mass Transfer 79 (2014) 796–806.

[8] H. Zhang, M. F. Modest, The full-spectrum correlated-k distribution for thermal radiation from molecular gas-particulate mixtures, Journal of Heat Transfer 124 (2002) 30–38.

[9] C. Wang, M. F. Modest, B. He, Full-spectrum k-distribution look-up table for nonhomogeneous gas-soot mixtures, Journal of Quantitative Spectroscopy & Radiative Transfer 176 (2016) 129–136.

[10] M. F. Modest, R. J. Riazzi, Assembly of full-spectrum k-distributions from a narrow-band database; effects of mixing gases, gases and nongray absorbing particles, and mixtures with nongray scatterers in nongray enclosures, Journal of Quantitative Spectroscopy & Radiative Transfer 90 (2005) 169–189.

[11] G. Pal, M. F. Modest, A Multiscale Full-Spectrum -Distribution Method for Radiative Transfer in Nonhomogeneous Gas-Soot Mixtures With Wall Emission, Computational Thermal Sciences 1 (2009) 137–158.

[12] G. Pal, M. F. Modest, A narrow band-based multiscale multigroup full-spectrum k-distribution method for radiative transfer in nonhomogenous gas-soot mixtures, Journal of Heat Transfer 132 (2010) 023307.

[13] V. P. Solovjov, B. W. Webb, Global Spectral Methods in Gas Radiation: The Exact Limit of the SLW Model and Its Relationship to the ADF and FSK Methods, J. Heat Transfer 133.

[14] B. W. Webb, V. P. Solovjov, F. Andre, An exploration of the influence of spectral model parameters on the accuracy of the rank correlated SLW model, Journal of Quantitative Spectroscopy and Radiative Transfer 218 (2018) 161–170.

[15] F. André, The l-distribution method for modeling non-gray absorption in uniform and non-uniform gaseous media, Journal of Quantitative Spectroscopy and Radiative Transfer 179 (2016) 19–32.

[16] F. André, An analysis of the symmetry issue in the -distribution method of gas radiation in non-uniform gaseous media, Journal of Quantitative Spectroscopy and Radiative Transfer 190 (2017) 78–87.

[17] P. Rivière, A. Soufiani, Updated band model parameters for H_2O, CO_2, CH_4 and CO radiation at high temperature, International Journal of Heat and Mass Transfer 55 (2012) 3349–3358.

[18] L. Pierrot, P. Rivière, A. Soufiani, J. Taine, A fictitious-gas-based absorption distribution function global model for radiative transfer in hot gases, J. Quant. Spectrosc. Radiat. Transfer 62 (1999) 609–624.

[19] S. P. Bharadwaj, M. F. Modest, A multiscale Malkmus model for treatment of inhomogeneous gas paths, Int. J. Therm. Sci. 46 (2007) 479–490.

[20] T. Ren, M. F. Modest, Line-by-Line Random-Number Database for Monte Carlo Simulations of Radiation in Combustion System, J. Heat Transfer 141.

[21] K. C. Tang, M. Q. Brewster, Analysis of Molecular Gas Radiation: Real Gas Property Effects, Journal of Thermophysics and Heat Transfer 13 (1999) 460–466.

[22] H. Chu, J. L. Consalvi, M. Gu, F. Liu, Calculations of radiative heat transfer in an axisymmetric jet diffusion flame at elevated pressures using different gas radiation models, Journal of Quantitative Spectroscopy and Radiative Transfer 197 (2017) 12–25.

[23] V. Kez, F. Liu, J. L. Consalvi, J. Ströhle, B. Epple, A comprehensive evaluation of different radiation models in a gas turbine combustor under conditions of oxy-fuel combustion with dry recycle, Journal of Quantitative Spectroscopy and Radiative Transfer 172 (2016) 121–133.

[24] J. Cai, R. Marquez, M. F. Modest, Comparisons of Radiative Heat Transfer Calculations in a Jet Diffusion Flame Using Spherical Harmonics and *k*-Distributions, Journal of Heat Transfer 136 (2014) 112702.

[25] F. Andre, F. R. Coelho, J.-L. Consalvi, F. H. R. Franca, M. Galtier, F. Nmira, V. P. Solovjov, B. W. Webb, Accuracy of engineering methods for radiative transfer in CO_2-H_2O mixtures at high temperature, in: Proceeding of Proceedings of the 9th International Symposium on Radiative Transfer, RAD-19, Begellhouse, Connecticut, 2019, pp. 407–414.

[26] J.-L. Consalvi, F. Andre, F. Coelho, F. Franca, M. Galtier, F. Nmira, V. Solovjov, B. Webb, Assessment of engineering gas radiative property models in high pressure turbulent jet diffusion flames, in: 9th International Symposium on Radiative Transfer, RAD-19, Athens, Greece, 2019.

[27] C. Wang, M. F. Modest, B. He, Full-spectrum correlated-k-distribution look-up table for use with radiative Monte Carlo solvers, International Journal of Heat and Mass Transfer 131 (2019) 167–175.

[28] A. Wang, M. F. Modest, Spectral Monte Carlo models for nongray radiation analyses in inhomogeneous participating media, Int. J. Heat and Mass Transfer 50 (2007) 3877–3889.

[29] M. Galtier, S. Blanco, J. Dauchet, M. El Hafi, V. Eymet, R. Fournier, M. Roger, C. Spiesser, G. Terrée, Radiative transfer and spectroscopic databases: A line-sampling Monte Carlo approach, Journal of Quantitative Spectroscopy and Radiative Transfer 172 (2016) 83–97. doi:10.1016/j.jqsrt.2015.10.016.

[30] M. Giles, F. Kudo, I. Sloan, B. Waterhouse, Quasi-monte carlo for finance applications, Journal of Australian Mathematical Society 50 (2008) 308–323.

[31] R. Ohbuchi, M. Aono, Quasi-Monte Carlo rendering with adaptive sampling, Tech. rep., IBM Tokyo Research Laboratory, http://www.kki.yamanashi.ac.jp/~ohbuchi/online_pubs/eg96_html/eg96.htm (1996).

[32] H. Niederreiter, Random Number Generation and Quasi-Monte Carlo Methods, Society for Industrial and Applied Mathematics, 1992.

[33] D. M. O'Brien, Accelarated quasi Monte Carlo integration of the radiative transfer equation, Journal of Quantitative Spectroscopy & Radiative Transfer 48 (1992) 41–59.

[34] A. Kersch, W. Morokoff, A. Schuster, Radiative heat transfer with quasi-Monte Carlo methods, Transport Theory and Statistical Physics 23 (1994) 1001–1021.

[35] A. J. Marston, K. J. Daun, M. R. Collins, Geometric optimization of radiant enclosures containing specularly-reflecting surfaces through quasi-Monte Carlo simulation, Numerical Heat Transfer, Part A: Applications 59 (2011) 81–97.

[36] Z. Wang, S. Cui, J. Yang, H. Gao, C. Liu, Z. Zhang, A novel hybrid scattering order-dependent variance reduction method for Monte Carlo simulations of radiative transfer in cloudy atmosphere, Journal of Quantitative Spectroscopy & Radiative Transfer 189 (2017) 283–302.

[37] X. Lu, P.-f. Hsu, Reverse Monte Carlo method for transient radiative transfer in participating media, Journal of Heat Transfer 126 (2004) 621–627.

[38] L. Palluotto, N. Dumont, P. Rodrigues, C. Koren, R. Vicquelin, O. Gicquel, Comparison of Monte Carlo methods efficiency to solve radiative energy transfer in high fidelity unsteady 3D simulations, in: ASME Turbo Expo 2017: Turbomachinery Technical Conference and Exposition, ASME, Charlotte, North Carolina, United States, 2017.

[39] M. Modest, D. Haworth, Radiative Heat Transfer in Turbulent Combustion Systems, Springer, 2015.

[40] P. Andreo, Monte carlo simulations in radiotherapy dosimetry, Radiation Oncology 13 (2018) 121.

[41] H. Ali, N. Firdous, S. Naz, F. Ghafoor, S. Saghir, Use of monte carlo methods in biomedical applications, 2015.

[42] T. Ren, M. F. Modest, Hybrid wavenumber selection scheme for line-by-line photon Monte Carlo simulations in high-temperature gases, ASME Journal of Heat Transfer 135 (8) (2013) 084501.

[43] S. K. Park, K. W. Miller, Random number generators: Good ones are hard to find, Communications of the ACM 31 (10) (1988) 1192–1201.

[44] F. James, A review of pseudoranom number generators, Computer Physics Communications 60 (1990) 329–344.

[45] L. Torvalds, Linux kernel documentation, accessed on Feb 08, 2019 (2019).
URL `https://git.kernel.org/pub/scm/linux/kernel/git/stable/linux.git/tree/drivers/char/random.c`

[46] W. H. Press, Numerical Recipes, University of Cambridge, 1986.

[47] H. Niederreiter, Quasi-monte carlo methods and pseudo-random numbers, American Mathematical Society 84 (1978) 957–1041.

[48] P. Brately, B. Fox, Algorith 659: Implementing Sobol's quasirandom sequence generator, ACM Transactions on Mathematical Software 14 (1988) 88–100.

[49] B. L. Fox, Algorithm 647: Implementation and relative efficiency of quasirandom sequence generators, ACM Transactions on Mathematical Software 12 (1986) 362–376.

[50] I. M. Sobol, Uniformly distributed sequences with an additional uniform property, USSR Computation Mathematics and Mathematical Physics 16 (1976) 236–242.

[51] I. A. Antonov, V. M. Saleev, An economic method of computing lpτ - sequences, USSR Computational Mathematics and Mathematical Physics 19 (1979) 252–256.

[52] J. Halton, On the efficiency of certain quasi-random sequences of points in evaluating multi-dimensional integrals, Numerische Mathematik 2 (1960) 84–90.

[53] S. Tezuka, Polynomial arithmetic analogue of {h}alton sequences, ACM Transactions on Modeling and Computer Simulation 3 (1993) 99–107.

[54] H. Niederreiter, Point sets and sequences with small discrepancy, Monatshefte fr Mathematik 104 (1987) 273–337.

[55] H. Niederreiter, Low-discrepancy and low-dispersion sequences, Journal of Number Theory 30 (1988) 51–70.

[56] A. Wang, M. F. Modest, Photon Monte Carlo simulation for radiative transfer in gaseous media represented by discrete particle fields, J. Heat Transfer 128 (2006) 1041–1049.

[57] L. S. Rothman, I. E. Gordon, R. J. Barber, H. Dothe, R. R. Gamache, A. Goldman, V. I. Perevalov, S. A. Tashkun, J. Tennyson, HITEMP, the high-temperature molecular spectroscopic database, Journal of Quantitative Spectroscopy & Radiative Transfer 111 (15) (2010) 2139–2150.

[58] Siemens, SGT-100, http://www.energy.siemens.com/us/en/fossil-power-generation/gas-turbines/sgt-100.htm.

[59] T. Ren, M. F. Modest, S. Roy, Monte Carlo Simulation for Radiative Transfer in a High-Pressure Industrial Gas Turbine Combustion Chamber, Journal of Engineering Gas Turbines and Power 140 (5) (2017) 051503.

[60] L. Pickett, C. Genzale, G. Bruneaux, L.-M. Malbec, L. Hermant, J. Shramm, Comparison of diesel spray combustion in different high-temperature, high pressure facilities, SAE International 3 (2010) 156–181.

[61] K. Mukut, S. P. Roy, A Sensitivity Study on Soot and NOx Formation in High Pressure Combustion System, in: 2018 Spring Technical Meeting of Central States Section of the Combustion Institute, Minneapolis, MN, USA, 2018.

[62] K. Mukut, S. Roy, An Investigation of Soot Evolution in High-pressure Spray Combustion, in: 11th US National Combustion Meeting, Pasadena, CA, 2019, pp. 1–9.

[63] H. Chang, T. T. Charalampopoulos, Determination of the wavelength dependence of refractive indices of flame soot, Proceedings of the Royal Society A 430 (1990) 577—-591.

[64] M. Klassen, J. P. Gore, Structure and radiation properties of pool fires, Tech. rep. (1994).

[65] B. Wu, X. Zhao, S. Roy, Detailed modeling of a small-scale turbulent pool fire, in: 11th US National Combustion Meeting, 2019, pp. 1–10.

[66] B. Wu, X. Zhao, S. Roy, A numerical study of radiation in a small-scale pool fire, in: The 9th International Symposium on Radiative Transfer (RAD-19), Athens, Greece, 2019.

[67] J. A. Farmer, S. P. Roy, An efficient Monte Carlo-based solver for thermal radiation in participating media, in: 4th Thermal and Fluids Engineering Conference, ASTFE, Las Vegas, NV, 2019.

Appendix A. Error bounds and standard deviation from MC and QMC

As discussed in Sec. 4, because QMC is based on a deterministic sequence (*i.e.*, an LDS will always produce the same sequence), calculation of standard deviation has so far been avoided. In order to estimate standard deviation one needs to make sure that the actual sequence of samples used in each QMC simulation is different. This is achieved, in a somewhat adhoc manner, by creating a six-dimensional Sobol sequence with $S \times N$ samples denoted as

$$\mathbf{S}_6 = [(\mathcal{S}_1^1, \mathcal{S}_1^2, \ldots, \mathcal{S}_1^6), (\mathcal{S}_2^1, \mathcal{S}_2^2, \ldots, \mathcal{S}_2^6), \ldots, (\mathcal{S}_{SN}^1, \mathcal{S}_{SN}^2, \ldots, \mathcal{S}_{SN}^6)] \tag{A.1}$$

Then m^{th} instance of QMC with N rays is run by using rays generated from the subset

$$[(\mathcal{S}_{(m-1)N+1}^1, \mathcal{S}_{(m-1)N+1}^2, \ldots, \mathcal{S}_{(m-1)N+1}^6), \ldots, (\mathcal{S}_{mN}^1, \mathcal{S}_{mN}^2, \ldots, \mathcal{S}_{mN}^6)],$$
$$m = [1, 2, \ldots, S] \tag{A.2}$$

Since any subset of an LDS is also LDS by definition, this m^{th} subset acts as a different (although not independent) LDS. It is possible to develop a more rigorous methodology of randomizing the LDS from one instance to another, but that has been left for future. This is somewhat similar to generating statistics from S different statistical iterations of PMC with N rays.

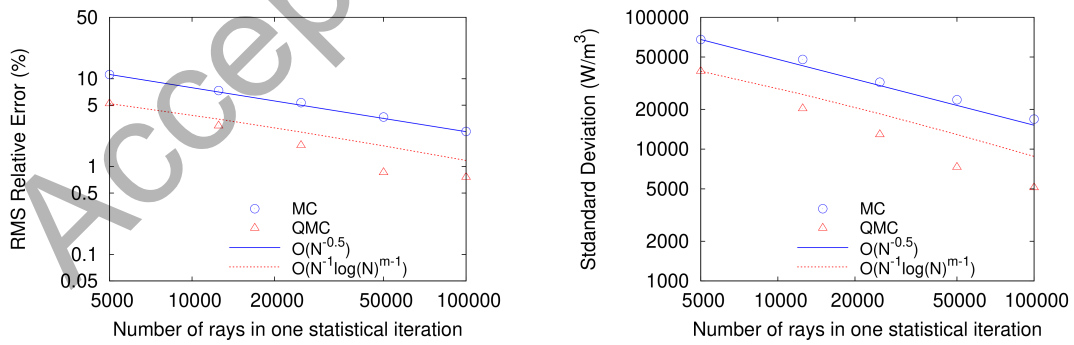

(a) Relative RMS error (b) Standard Deviation

Figure A.20: Convergence rate of RMS error and standard deviation for one-dimensional plane-parallel media (Case 3). Both MC and QMC (using Sobol) was run for 10 statistical iterations. The dimension for Sobol sequence is $m = 6$.

Figure A.20 shows the results from series of such simulations with different number of rays per statistical iteration ($N = [5000, 100000]$) for the one-dimensional nongray case (Case 3 in Tab. 1). Here only results from Sobol sequence is shown. Both MC and QMC were run for $S = 10$. As before the relative RMS error is calculated from the analytical solution. Both the relative RMS error (Fig. 20(a)) and absolute value of standard deviation (Fig. 20(b)) are shown here. It is evident that both the standard deviation and error reduces faster for QMC than MC. It can be shown that the probabilistic *error bound* for a Monte Carlo solution is expected to vary with number of samples as $O\left(N^{-0.5}\right)$, whereas that for QMC varies as $O\left(N^{-1}\left(\log N\right)^{m-1}\right)$, where m is the dimension of the LDS (*i.e.*, in current case, $m = 6$) [32]. The lines corresponding these error bounds are also shown in corresponding figures. Clearly the error as well as the standard deviation of MC decreases as per $O\left(N^{-0.5}\right)$. However, it is interesting to observe that both the error and standard deviation from QMC decreases faster than $O\left(N^{-1}\left(\log N\right)^{m-1}\right)$. As expected, both the error and standard deviation show the same rate of decrease with sample size in either MC or QMC. Therefore, either of these two metric can be used to define a "convergence rate." It is noted here that the error bound of QMC is dependent on the dimensionality of the problem. If one can reduce the dimensionality, it is expected the QMC may lead to an even faster convergence rate. Therefore, combination QMC with a reasonably accurate spectral model such as FSK or SLW or l-distribution may lead to further speed-up of QMC because of the elimination of the need for a quasirandom number for wavenumber selection.

Finally, Fig. A.21 shows the comparison of RMS relative error and standard deviation from MC and QMC (with Sobol sequence) for the gas turbine case. MC was run for $S = 10$ independent statistical iterations with $N = 1,600,000$ rays in each iteration and QMC were run with $S = 10$ different sub-intervals with $N = 1,600,000$ rays in each interval. Only the results along the $r = 0.03$ m line is shown here and the error is calculated based on the benchmark run as discussed in Sec. 4.2.1. Both the error and standard deviation is much lower from QMC than MC. The computational time for both MC and QMC is similar (as both cases use a total of 1.6×10^7 rays split in 10 iterations). This comparison shows why FoM benefit from QMC is always more than S-fold from MC with S statistical iterations.

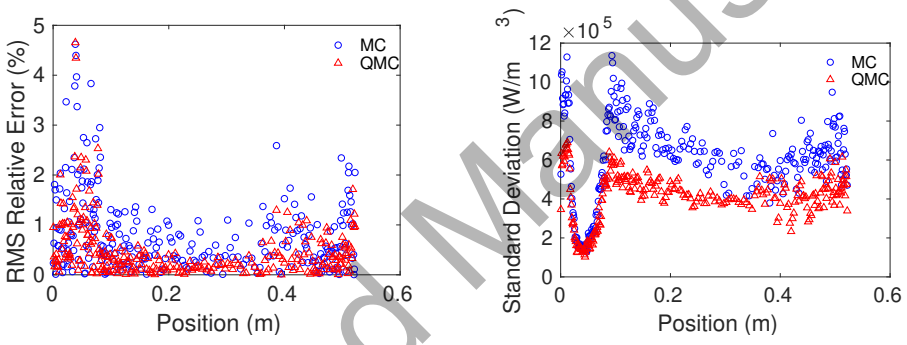

(a) Relative RMS error (b) Absolute value of standard deviation

Figure A.21: Relative RMS error and standard deviation for radiative absorption along $r = 0.03$ m in the gas turbine case. Both MC and QMC (using Sobol) was run 10 statistical iterations with 1,600,000 rays in each iterations.